Science Advances
AAAS

advances.sciencemag.org/cgi/content/full/6/13/eaay5986/DC1

Supplementary Materials for

Soft crystal martensites: An in situ resonant soft x-ray scattering study of a liquid crystal martensitic transformation

Hyeong Min Jin, Xiao Li, James A. Dolan, R. Joseph Kline, José A. Martínez-González, Jiaxing Ren, Chun Zhou, Juan J. de Pablo, Paul F. Nealey*

*Corresponding author. Email: nealey@uchicago.edu

Published 27 March 2020, *Sci. Adv.* **6**, eaay5986 (2020)
DOI: 10.1126/sciadv.aay5986

The PDF file includes:

Other Supplementary Material for this manuscript includes the following:

(available at advances.sciencemag.org/cgi/content/full/6/13/eaay5986/DC1)

Supplementary Notes

Note S1. Misaligned BP domains

Despite using chemical patterns to direct the growth of only a single BPII domain, it seems that within the region of the sample probed by our X-ray beam, another $BPII_{(100),\,45^\circ}$ domain is present which has an in-plane angle difference of 45°. As shown in **Fig. S2A** below, due to the polarization of the X-ray beam, the horizontal peaks of this domain $(01\bar{1})$ and $(0\bar{1}1)$ appear, but $(0\bar{1}\bar{1})$ and (011) are not captured. The $BPII_{(100),\,45^\circ}$ also underwent a martensitic transformation as the temperature decreases, forming another four sets of $BPI_{(110)}$ (**Fig. S2B**). This allows us to index some scattering peaks that were not indexed in **Fig. 4b** in the main text. However, the intensity of these peaks are low and they do not overlap with the peaks of the dominantly aligned BPII and BPI. Therefore, these peaks from $BPII_{(100),\,45^\circ}$ can safely be neglected when analyzing the RSoXS patterns.

Note S2. Continuum simulations

For the theoretical description of blue phases, we rely on the mean field Landau-de Gennes approach. In this context, the free energy, *F*, of the liquid crystal is given as follows (25),

$$F(\boldsymbol{Q}) = \frac{A}{2}\left(1-\frac{U}{3}\right)\,\mathrm{tr}(\boldsymbol{Q}^2) - \frac{AU}{3}\mathrm{tr}(\boldsymbol{Q}^3) + \frac{AU}{4}\mathrm{tr}(\boldsymbol{Q}^2)^2 + \frac{L}{2}\left[\left(\frac{\partial Q_{ij}}{\partial x_k}\right)^2 + 2q_0\epsilon_{ikl}Q_{ij}\frac{\partial Q_{lj}}{\partial x_k}\right] + f_s \qquad \text{(S1)}$$

where Q_{ij} are the components of the tensor order parameter, *A* and *U* are phenomenological parameters that depend on temperature and pressure, $q_0 = 2\pi/p$ is the inverse of the pitch (*p*), *L* is the elastic constant and ε_{ikl} is the Levi-Civita tensor. The last term of Eq. 1 corresponds to the surface contributions to the free energy, its form depends on the kind of anchoring conditions that are implemented. For planar degenerate anchoring we have (26),

$$f_S^{\mathrm{P}} = W_{\mathrm{P}}\left(\widetilde{\boldsymbol{Q}} - \widetilde{\boldsymbol{Q}}^{\perp}\right)^2, \qquad \text{(S2)}$$

where W_{P} represents the anchoring strength, $\widetilde{\boldsymbol{Q}} = \boldsymbol{Q} + S\boldsymbol{I}/3$ and $\widetilde{\boldsymbol{Q}}^{\perp} = \boldsymbol{P}\widetilde{\boldsymbol{Q}}\boldsymbol{P}$, where $P_{ij} = \delta_{ij} - \nu_i\nu_j$, where $\boldsymbol{\nu}$ is the vector normal to the surface. For homeotropic anchoring,

$$f_S^{\mathrm{H}} = \frac{W_{\mathrm{H}}}{2}(\boldsymbol{Q} - \boldsymbol{Q}_{\mathrm{o}})^2, \qquad \text{(S3)}$$

where $\mathbf{Q}_{\mathrm{o}}$ represents the preferred alignment at the surface. Minimization of the free energy, which leads to metastable and stable states, was achieved by means of a Ginzburg-Landau relaxation method over a lattice array with a mesh resolution of 7.5 nm as explained in reference (22) and (25).

For the description of the system we consider a chiral liquid crystal with pitch of 258 nm and the following phenomenological parameters that have been found to match experimental observations: $A = 1.067 \times 10^5$ J/m^3, L=6 pN, U = 2.755 for the initial BPII and U = 3.5 for the reference BPI. For anchoring energies, we consider $W_{\mathrm{P}} = W_{\mathrm{H}} = 1 \times 10^{-3}$ J/m^2. The BPII-BPI transformation was achieved as follows: first a $BPII_{(100)}$ was equilibrated, then the thermal parameter *U* was slowly changed up to the system reached the BPI regimen, we let the system relax to the equilibrium after each change of *U*, additional details can be found in reference (6).

Note S3. Lattice strain calculation during the martensitic transformation

The unit cell deformation accompanying the martensitic transformation from $BPII_{(100)}$ to $BPI_{(110)}$ can be described by the combined application of equal and opposite normal strains followed by an in-plane rotation of the lattice. **Fig. S4** shows the model system introduced to describe the two-dimensional lattice transformation from $BPII_{(100)}$ to $BPI_{(110)}$, as viewed along the *z*-axis. The contraction along the *b*-axis and the elongation along the *c*-axis required to transform $BPII_{(100)}$ to $BPI_{(110)}$ (**Fig. S4A**) is given by

$$S_{\mathrm{BPI}} = \begin{Bmatrix} -0.172 \\ 0.172 \\ 0 \end{Bmatrix}, \tag{S4}$$

where the values of ϵ_b and ϵ_c, equal in magnitude and opposite in sign, are based on the average values of those strain components as measured at the beginning of the martensitic transformation (**Table S1**). Since the $\{011\}_{\mathrm{BPII}}$ and $\{112\}_{\mathrm{BPI}}$ planes are parallel to one another and must maintain a similar *d*-spacing upon transformation, an in-plane rotation (θ = -9.75°) must also be applied during the phase transformation (**Fig. S4B**). To transform the strain values from the local (unit cell) to the global (macroscopic) coordinate system, a transformation matrix is used (27), such that

$$S' = \begin{Bmatrix} \epsilon'_x \\ \epsilon'_y \\ \gamma'_{xy} \end{Bmatrix} = \begin{bmatrix} \cos^2\theta & \sin^2\theta & \sin\theta\cos\theta \\ \sin^2\theta & \cos^2\theta & \sin\theta\cos\theta \\ -2\sin\theta\cos\theta & 2\sin\theta\cos\theta & \cos^2\theta - \sin^2\theta \end{bmatrix} \begin{Bmatrix} \epsilon_b \\ \epsilon_c \\ \gamma_{bc} \end{Bmatrix}. \tag{S5}$$

Using this transformation matrix, applying an in-plane rotation of -9.75° results in the following strain values:

$$S'_{-9.75^\circ} = \begin{Bmatrix} -0.162 \\ 0.162 \\ -0.115 \end{Bmatrix}. \tag{S6}$$

Similarly, the strain values of the other, differently oriented $BPI_{(110)}$ lattices with three different in-plane rotations may be calculated as follows:

$$S'_{-80.25^\circ} = \begin{Bmatrix} 0.162 \\ -0.162 \\ -0.115 \end{Bmatrix}, S'_{9.75^\circ} = \begin{Bmatrix} -0.162 \\ 0.162 \\ 0.115 \end{Bmatrix}, \text{ and } S'_{80.25^\circ} = \begin{Bmatrix} -0.162 \\ -0.162 \\ 0.115 \end{Bmatrix}. \tag{S7}$$

Note S4. Transformation pathway with shear strain

As we mentioned in the main text and in **Fig. 4C**, the planes $(011)_{\mathrm{BPII}} \parallel (1\bar{1}2)_{\mathrm{BPI}}$ are easily identified in the RSoXS scattering patterns during the martensitic transformation. As the X-rays are incident along the *z*-direction, lattice distortion in the *z*-direction cannot readily be analyzed using the current RSoXS geometry. However, due to the out-of-plane confinement imposed by the "sandwich" cell geometry, we assume that there will be no lattice change in the *z*-direction. Under this assumption, $[\bar{1}10]_{\mathrm{BPII}}$ and $[1\bar{1}\bar{1}]_{\mathrm{BPI}}$ are necessarily parallel, i.e. $[\bar{1}10]_{\mathrm{BPII}} \parallel [1\bar{1}\bar{1}]_{\mathrm{BPI}}$

(**Fig. S5A**). Therefore, the crystallographic orientation relationship between two phases is

$$(011)_{\text{BPII}} \parallel (1\bar{1}2)_{\text{BPI}}$$
$$[\bar{1}10]_{\text{BPII}} \parallel [1\bar{1}\bar{1}]_{\text{BPI}} \quad \text{(S8)}$$

We have already provided details of the transformation path—a normal strain along the *a* and *c* axes and an *xy* in-plane rotation (discussion section, Page 8 of the main text). It should be noted that, as the X-rays are incident along the *z*-direction in our RSoXS geometry, only shear strain on the *xy*-plane can be analyzed. As shown in the **Fig S5A**, during the transformation from BPII to BPI the $(011)_{\text{BPII}}$ plane behaves as an undistorted plane, and the shear strain occurs along the $[\bar{1}10]_{\text{BPII}}$ direction. The shear strain, γ along the $[\bar{1}10]_{\text{BPII}}$ direction can then be calculated as

$$\gamma = \frac{S}{h} \approx \tan\phi \quad \text{(S9)}$$

where *S* is the shear displacement relative to the undistorted plane, *h* is the distance between the shearing point and the undistorted plane, and φ is the angle caused the shear strain (**Fig. S5B**). From the RSoXS scattering pattern, and angle φ of ~19.5° is obtained. Thus, instead of determining *S*, and *h*, the crystallographic shear is approximately calculated by $\gamma \approx \tan\varphi$

$$(011)_{\text{BPII}}, [\bar{1}10]_{\text{BPII}}$$
$$\gamma = 0.354 \quad \text{(S10)}$$

We can provide an alternative description of twin formation based on the previously determined shear strain. As we mentioned above, during the martensitic transformation, there is the shear strain in the system (**Fig. S5B**). Therefore, to compensate the shear strain during the transformation and prevent bulk motion, twin formation is necessary. From the RSoXS scattering pattern, we confirmed is the presence of the twin phase, which shares the undistorted planes (**Fig. S5C**). The shear strain from twin formation, γ_{twin} along the $[1\bar{1}0]_{\text{BPII}}$ direction can then be calculated as

$$\gamma_{\text{twin}} = \frac{2S}{h} \approx \tan\psi \quad \text{(S11)}$$

where ψ is the angle caused by the twin formation and equals to 2φ. From the RSoXS scattering pattern, angle ψ of ~39.0° is obtained. Therefore, instead of determining *S*, and *h*, the crystallographic shear from the twinning approximately calculated with ψ

$$(011)_{\text{BPII}}, [\bar{1}10]_{\text{BPII}} \text{ or } (1\bar{1}2)_{\text{BPI}}, [1\bar{1}\bar{1}]_{\text{BPI}}$$
$$\gamma_{\text{twin}} = -0.707 \text{ or } \gamma_{\text{twin, on BPII}} = -0.354 \quad \text{(S12)}$$

where γ_{twin} is the shear strain from the twin formation ($= 2S/h \approx \tan\psi$, i.e. based on the transformed BPI), and $\gamma_{\text{twin, on BPII}}$ is the twinning shear strain based on the parent BPII lattice ($= S/h \approx \tan\varphi$). It should be noted that the negative sign of the $[\bar{1}10]_{\text{BPII}}$ shear strains is due to the shear direction, which is opposite to that of $[1\bar{1}0]_{\text{BPII}}$. Therefore, based on the parent BPII lattice, the shear strain from twinning is -0.354, which is the same magnitude and opposite direction as the shear strain caused by the martensitic transformation. Therefore, if the transformed BPI

phase and the twin phase exist in the same proportions, the shear strain incurred by the martensitic transformation will be canceled out.

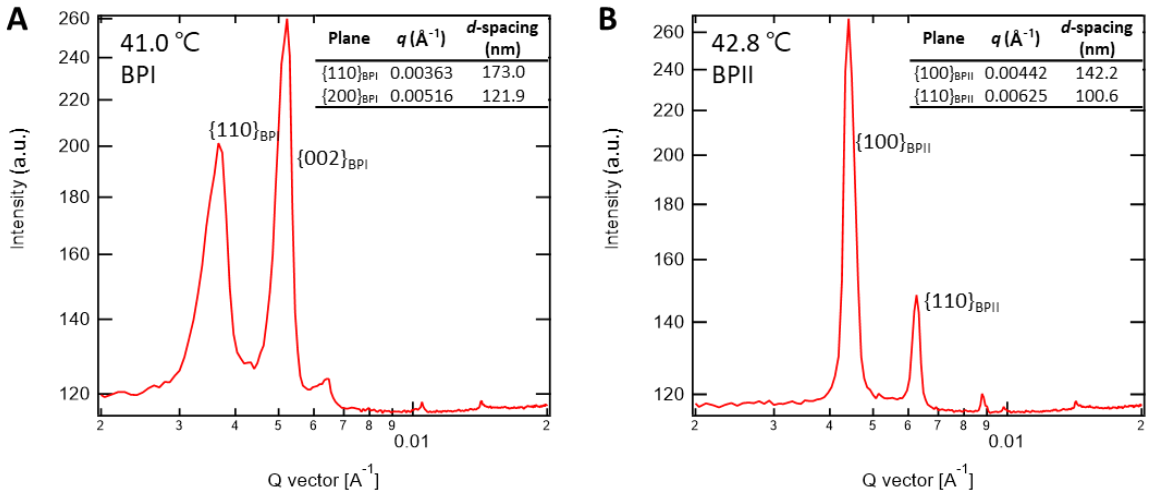

Fig. S1. RSoXS intensity profiles of BPI and BPII during heating. (**A**) BPI at 41.0 °C and (**B**) BPII at 42.8 °C. Inset tables show the *q*-values and their *d*-spacing.

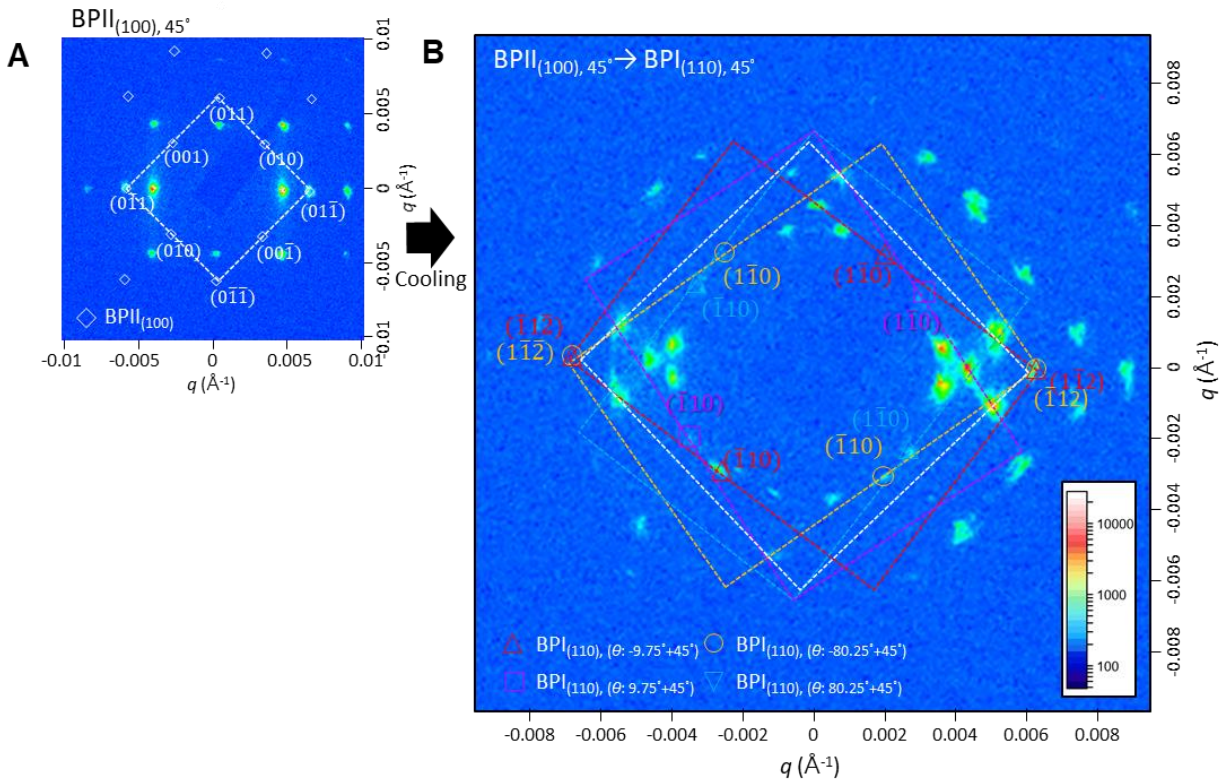

Fig. S2. RSoXS peak indexing of misaligned domains. (**A**) $BPII_{(100),\ 45^{\circ}}$ at 43.0 °C and (**B**) polycrystalline $BPI_{(110),\ 45^{\circ}}$ at 40.7 °C, which is transformed from $BPII_{(100),\ 45^{\circ}}$ and possesses a distinct set of poly-crystals with four different in-plane orientations.

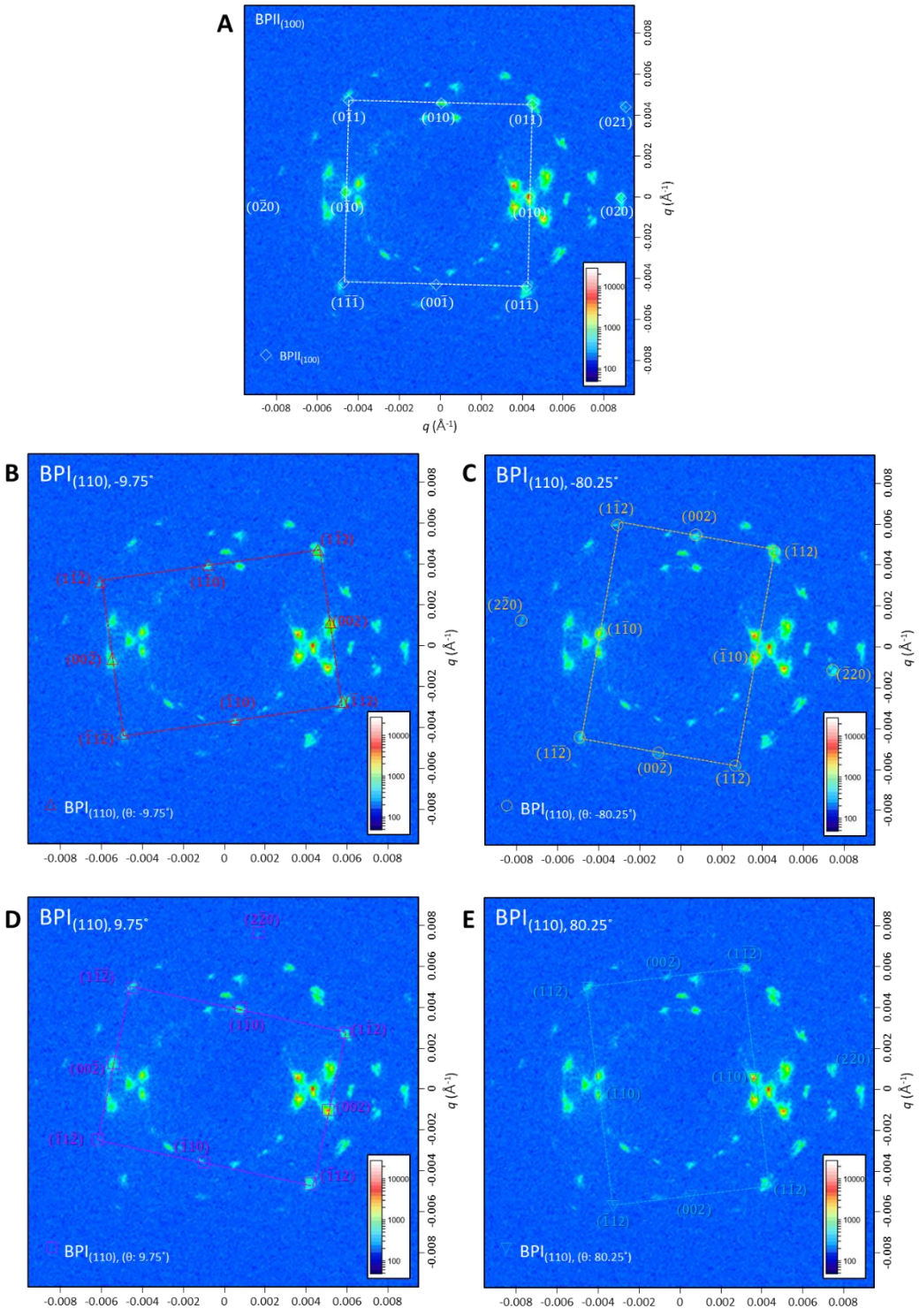

Fig. S3. RSoXS peak indexing during the BPII to BPI martensitic transformation. (**A**) $BPII_{(100)}$, (**B**) $BPI_{(110),\ -9.75°}$, (**C**) $BPI_{(110),\ -80.25°}$, (**D**) $BPI_{(110),\ 9.75°}$, and (**F**) $BPI_{(110),\ 80.25°}$ at 40.7 °C.

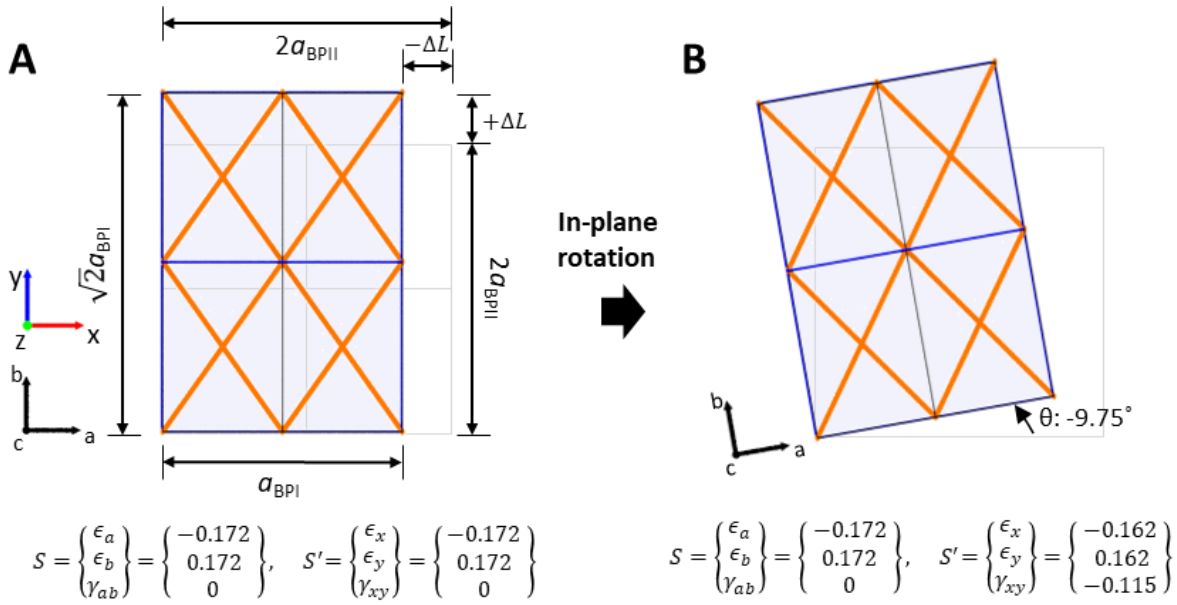

Fig. S4. Model system for the lattice transformation from BPII$_{(100)}$ to BPI$_{(110)}$. Total lattice deformation on *xy*-plane during the transformation consists of (**A**) normal strain and (**B**) in-plane rotation.

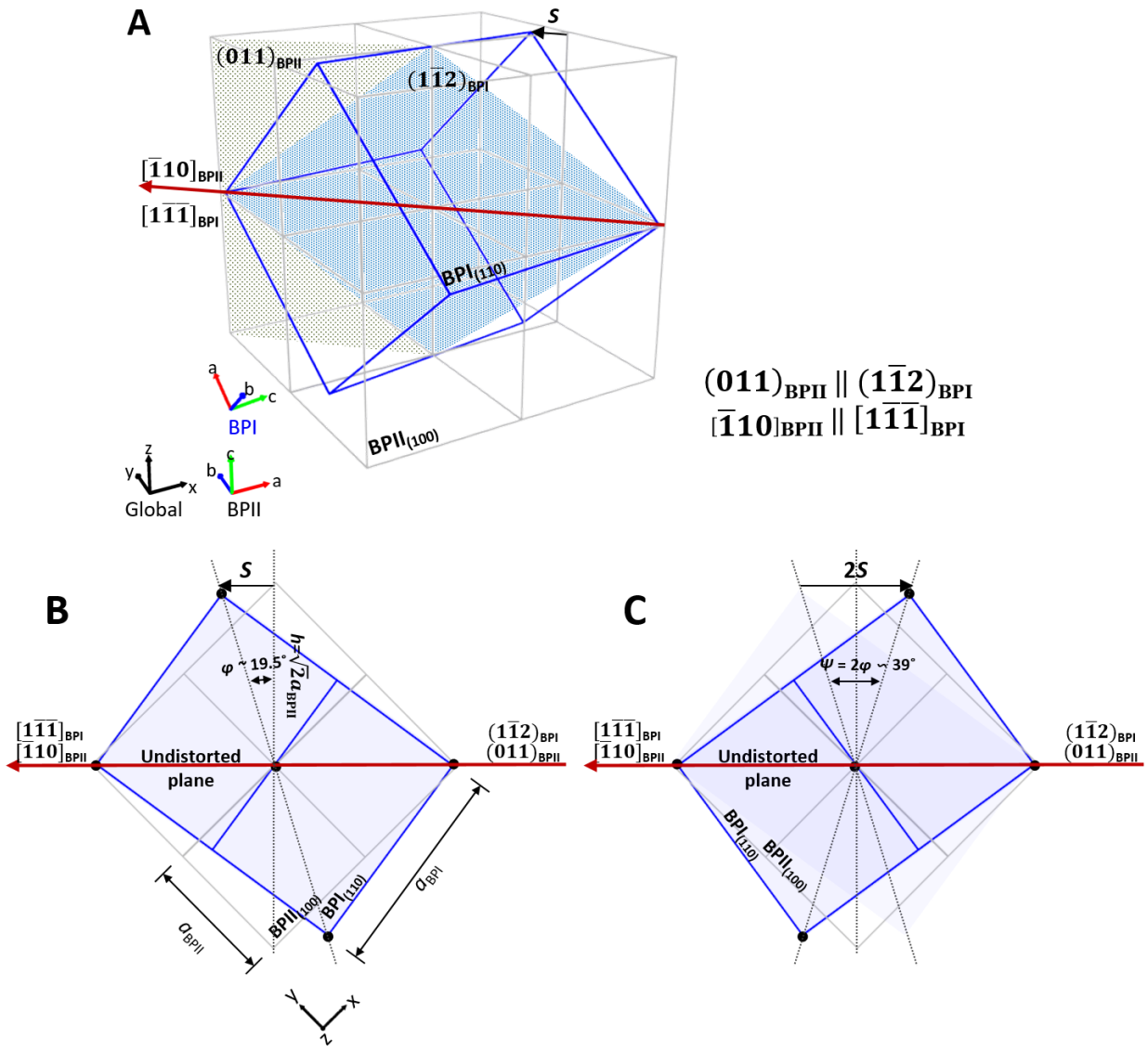

Fig. S5. Transformation pathway with shear strain. (**A**) Crystallographic orientation relationship between BPII and BPI during martensitic transformation. The shear displacement, *S*, is shown as the black arrow; the shaded gray and blue planes are the $(011)_{BPII}$ and $(\mathbf{1\bar{1}2})_{BPI}$ planes, respectively; and the gray and blue outlines highlight the position of BPII and BPI unit cells, respectively. (**B**) Their projection onto the *xy*-plane and (**C**) their twin phase (Twin mode: $(\mathbf{1\bar{1}2})_{BPI}$, $[\mathbf{1\bar{1}\bar{1}}]_{BPI}$).

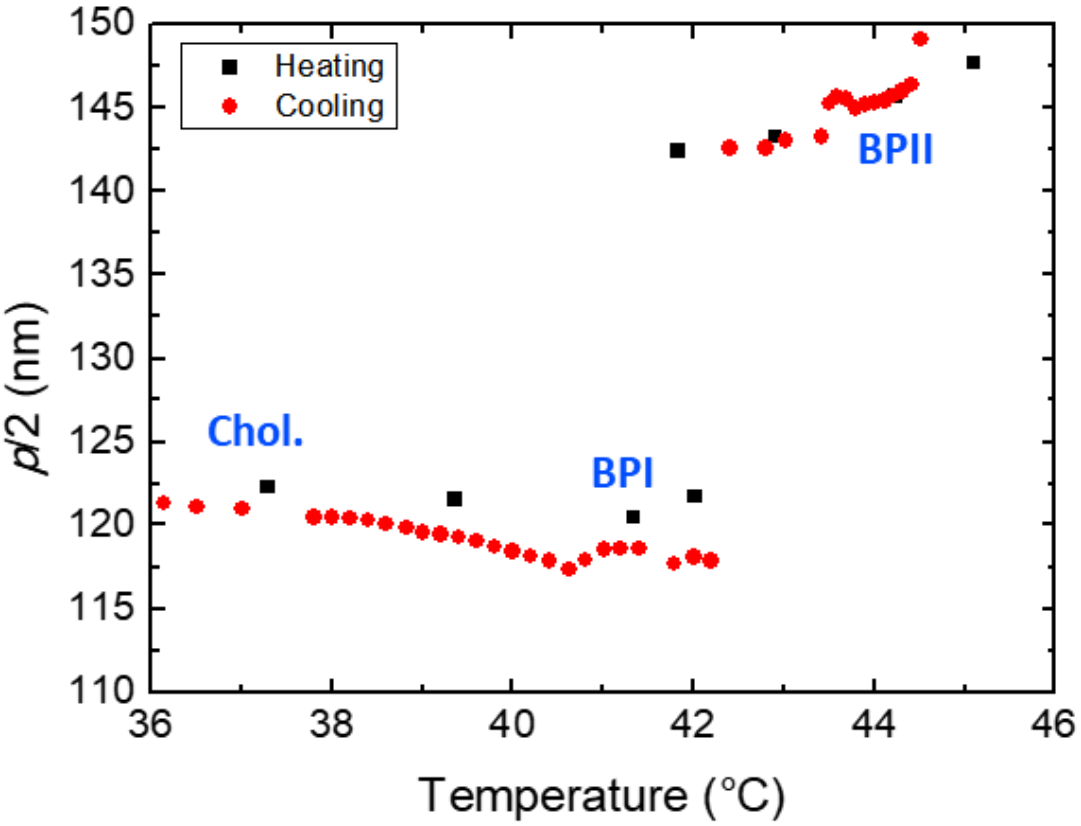

Fig. S6. Variation in half-pitch length (*p*/2) of chiral nematic during heating and cooling. The lattice constants of BPI and BPII should correspond to full-pitch, *p* and half-pitch *p*/2 respectively.

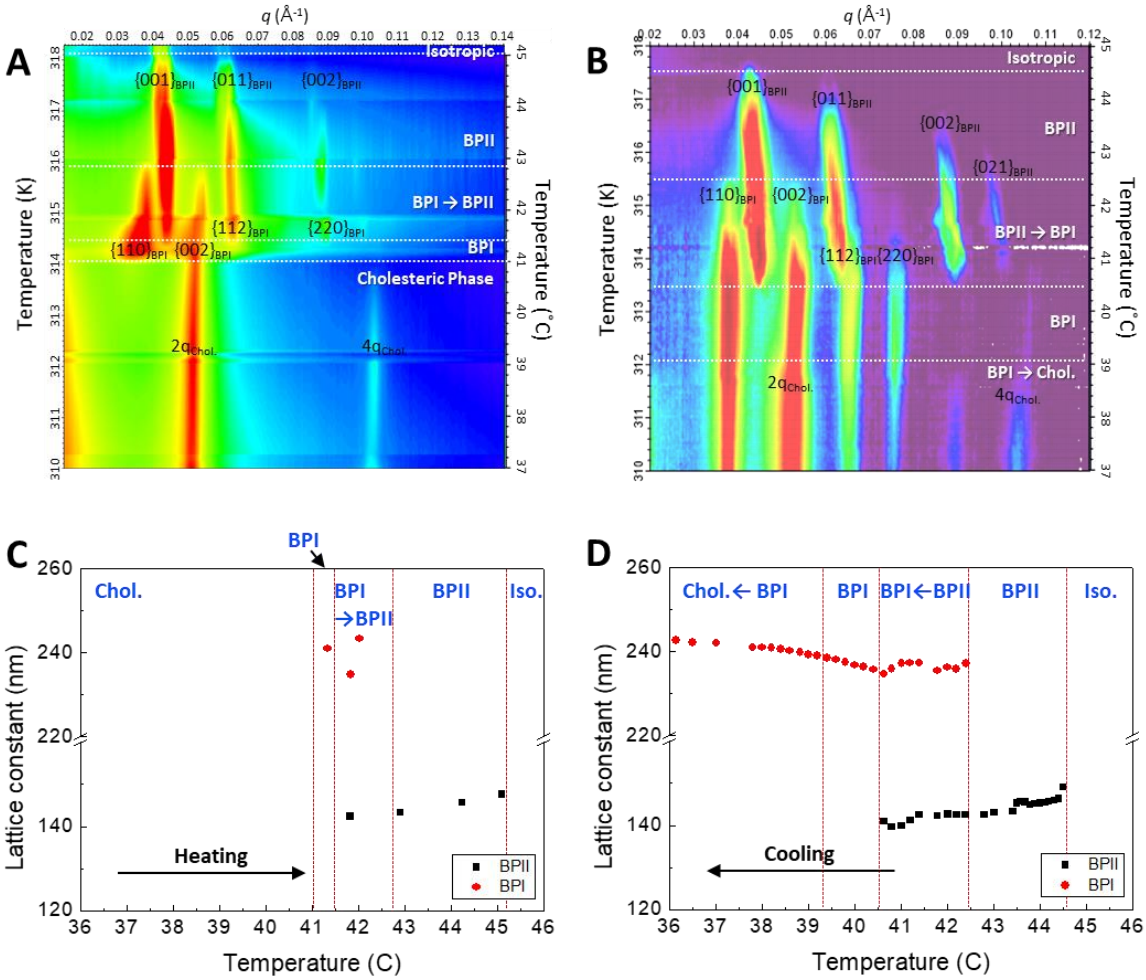

Fig. S7. The evolution of the scattering intensity and corresponding lattice constant during heating and cooling. The scattering intensity during (**A**) heating and (**B**) cooling and variation of lattice constants during (**C**) heating and (**D**) cooling.

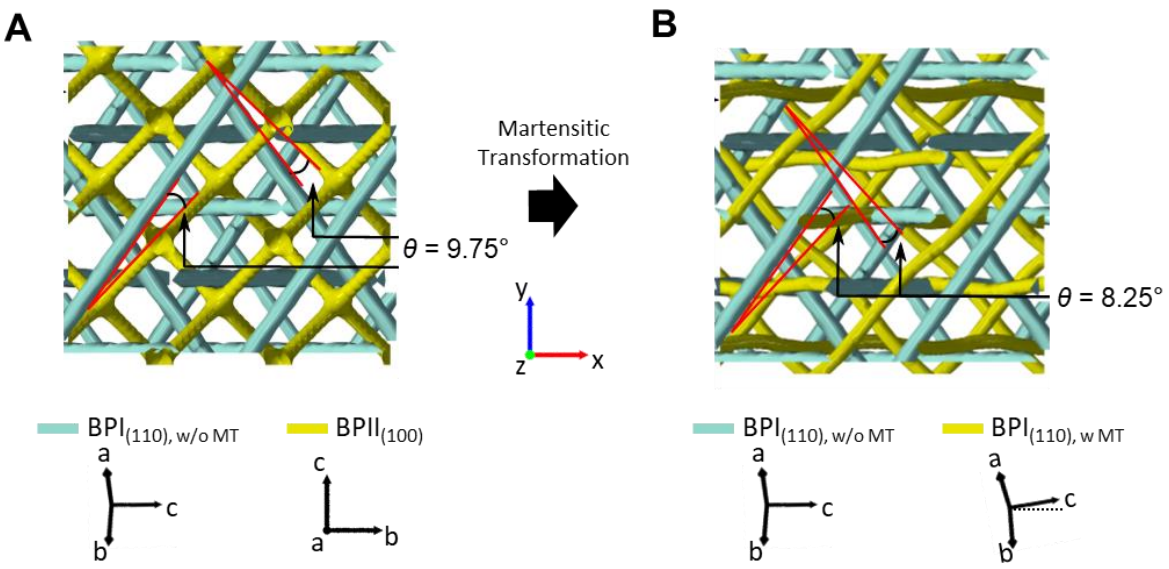

Fig. S8. Reconfiguration of disclination network during the martensitic transformation from BPII to BPI. (**A**) 2D projection on the *xy*-plane of the initial $BPII_{(100)}$ and a reference $BPI_{(100)}$ where both crystals share the same local coordinate frame. Our simulations suggest that the angle between the projected disclinations lines is the origin of the in-plane of the forming BPI. (**B**) The $BPI_{(110)}$ that is formed from the martensitic transformation shows an in-plane rotation of 8.25° respect to the reference experimental frame.

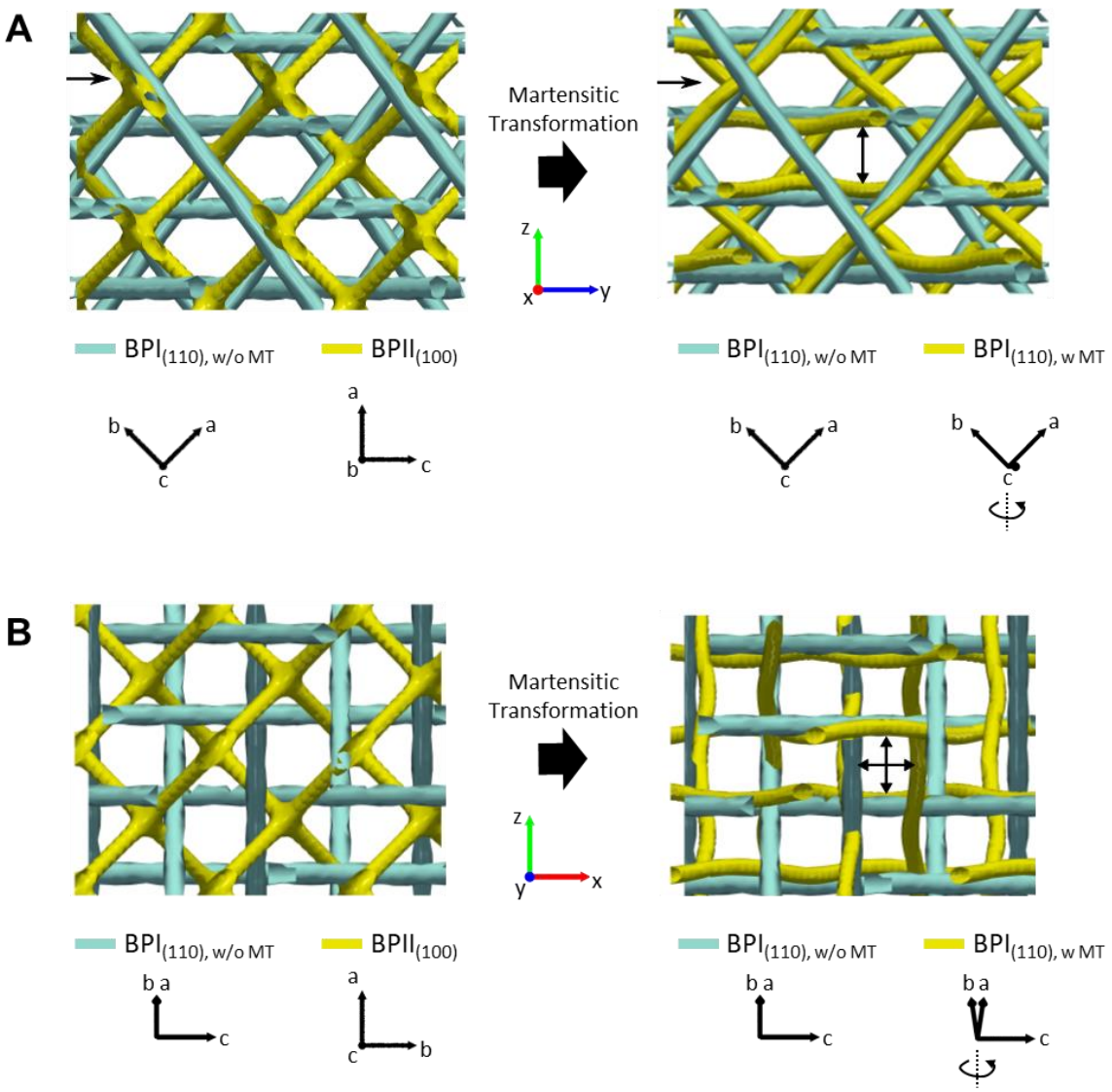

Fig. S9. Reconfiguration of disclination network on the *yz* and *xz* plane. 2D projections of the initial BPII(100) and the reference $BPI_{(100)}$ on the (**A**) *yz*- and (**B**) *xz*- planes. The $BPI_{(100)}$ formed from the BPII has a smaller (~4 %) unit cell than the reference cubic BPI as indicated by the inset arrows.

Table S1. Measured *d*-spacing and strain components of $BPI_{(110)}$ lattices at the beginning of the martensitic transformation from $BPII_{(100)}$. ϵ_b and ϵ_c are the normal strain component in their lattice coordination and ϵ_x, ϵ_y, and γ_{xy} are the strain components in the *xy* global coordination (i.e. lattice coordination of parent $BPII_{(100)}$).

Lattice	θ (°)	$d_{100,\,BPII}$ (nm)	$d_{110,\,BPI}$ (nm)	$d_{200,\,BPI}$ (nm)	ϵ_b	ϵ_c	ϵ_x	ϵ_y	γ_{xy}
$BPII_{(100)}$		141.1			0	0	0	0	0
$BPI_{(110),\,-9.75^\circ}$	-9.52		164.1	116.9	-0.171	0.163	-0.162	0.154	-0.109
$BPI_{(110),\,-80.25^\circ}$	-80.77		163.3	117.1	-0.170	0.157	0.149	-0.162	-0.104
						Twin 1	**-0.007**	**-0.004**	**-0.107**
$BPI_{(110),\,9.75^\circ}$	10.55		166.4	117.7	-0.166	0.179	-0.154	0.168	0.124
$BPI_{(110),\,80.25^\circ}$	81.3		164.6	118.4	-0.161	0.166	0.159	-0.153	0.098
						Twin 2	**0.002**	**0.007**	**-0.111**
Average					**-0.167**	**0.167**	**-0.002**	**0.002**	**0.002**

Movie S1. Reconfiguration of disclination network during martensitic transformation. This video shows the reconfiguration of disclination network during martensitic transformation from $BPII_{(100)}$ to $BPI_{(110)}$. The reconfiguration is observed on the *xy*-plane to apparently show the in-plane rotation during the martensitic transformation.